Available online at www.sciencedirect.com
SCIENCE DIRECT
Journal of Catalysis 238 (2006) 250–259
JOURNAL OF CATALYSIS
www.elsevier.com/locate/jcat

Utilizing full-exchange capacity of zeolites by alkaline leaching: Preparation of Fe-ZSM5 and application in N_2O decomposition

I. Melián-Cabrera [a,*], S. Espinosa [b], J.C. Groen [b], B. v/d Linden [b], F. Kapteijn [b,*], J.A. Moulijn [b]

[a] *Dept. Chemical Engineering, Stratingh Institute, University of Groningen, Nijenborgh 4, 9747 AG Groningen, The Netherlands*
[b] *R&CE, DelftChemTech, Delft University of Technology, Julianalaan 136, 2628 BL Delft, The Netherlands*

Received 24 August 2005; revised 13 November 2005; accepted 15 November 2005

Available online 18 January 2006

Abstract

Utilization of the full exchange capacity of zeolites has been achieved by shortening diffusional lengths on a mild alkaline leaching treatment. Iron was fully incorporated by liquid-phase ion exchange on ZSM5 without the formation of Fe-oxides, leading to improved activity in the N_2O-decomposition reaction. It is demonstrated that the large crystal size of the zeolite dominates the Fe^{III}-exchange process. The crystallinity of the ZSM5 zeolite can be tuned down by postsynthesis modification of commercial samples by caustic leaching. Under the study conditions, two phenomena were observed: (i) The size of the zeolite agglomerates is significantly reduced while the microporosity is preserved, and (ii) at prolonged treatment, an additional mesopore network is created. The mesopores display a wide pore size distribution with randomly organized mesopores. The MFI lattice is well preserved in both cases. Based on the characterisation data and activity results, it is concluded that deagglomeration of the zeolite crystals enables full exchange. The newly created mesopores at harsher conditions are not responsible for the improved exchange. At short leaching times, full-exchange loading of Fe^{III} is achieved (and negligible inactive FeO_x), leading to a considerable enhancement of the activity for N_2O decomposition. Mesopore formation does not further improve the performance of N_2O decomposition. From the activity increase, it is concluded that a "fraction" of the extra Fe becomes active, which increases with the exchange degree.

Keywords: N_2O decomposition; Zeolite ion-exchange; Desilication; Caustic washing; Alkali treatment; Postsynthesis modification; Mesopore formation; Alkali treatment; ZSM5

1. Introduction

Zeolite-based catalysts have proven industrial possibilities for redox reactions. The use of Fe-MFI systems for direct N_2O decomposition has been described in several publications [1–4]. Fe-ZSM5 catalysts have also attracted much attention due to their extraordinary activity for hydrocarbon-assisted reduction of N_2O [5,6], N_2O reduction by NH_3 [7], oxidation of benzene to phenol (Panov's group [8]), and selective catalytic reduction (SCR) of NO_x with hydrocarbons [9–12] and NH_3 [13].

There has been increasing interest in Fe-ZSM5 catalysts, especially in attempts to prepare "overexchanged" catalysts. Alternative procedures to the approach of Feng and Hall [9,10,14] have been investigated in gas-phase [15–21], solid-state [11,12,22], and aqueous ion exchange using different types of Fe-salt solutions [13–27]. Sublimation of $FeCl_3$ results in Fe loadings as high as $Fe/Al = 1$, but it is generally observed that after washing and calcination iron is clustered to inactive FeO_x [28]. Alternatively, Pérez-Ramírez et al. reported a preparation method based on poststeamed isomorphously substituted Fe-ZSM5 zeolite [29]. Although this method lacks flexibility in Fe loading, a small fraction of Fe (typically 0.5 wt%) yields excellent performance for N_2O decomposition.

In industrial applications, aqueous or wet ion exchange (WIE) is the simplest methodology, because it involves fewer steps and the process parameters (e.g., pH, temperature, concentration) are easily accessible. However, during preparation of Fe-ZSM5 by WIE, we have systematically achieved less than half of the full exchange capacity. Studies addressing this problem are scarce or partially overlooked in the literature.

* Corresponding authors.
E-mail addresses: i.v.melian.cabrera@rug.nl (I. Melián-Cabrera), f.kapteijn@tnw.tudelft.nl (F. Kapteijn).

0021-9517/$ – see front matter
doi:10.1016/j.jcat.2005.11.034

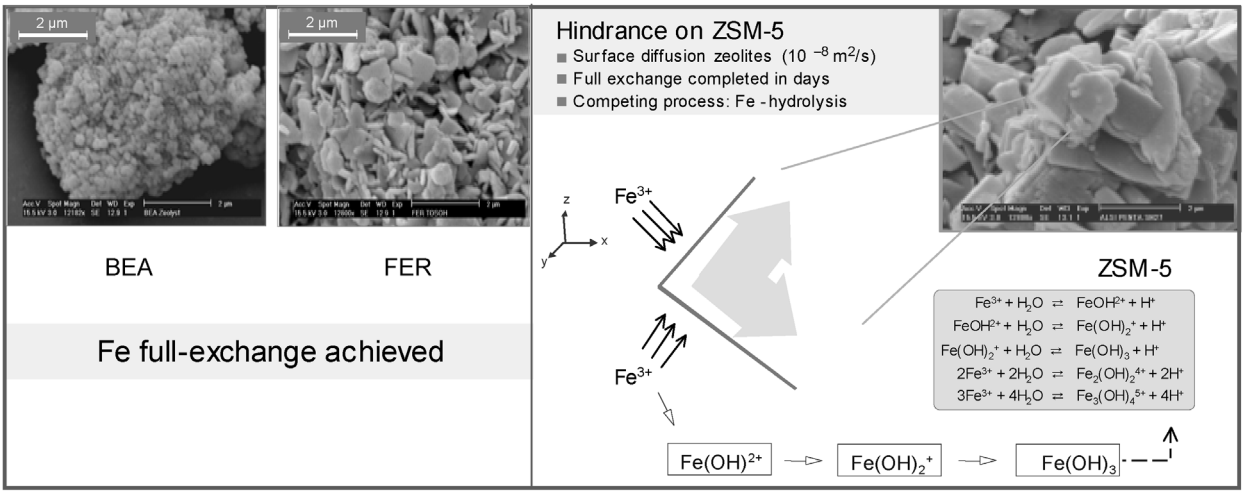

Fig. 1. (Right) Problem definition. Large crystal size combined with the surface diffusion in zeolites makes the exchange process rather slow. Fe^{III} hydrolysis to inactive $Fe(OH)_3$ simultaneously competes. (Left) This is confirmed with exchange experiments with BEA and FER, where a complete exchange is achieved.

This problem stems from the zeolite crystal size. The zeolite's agglomerates, depicted in Fig. 1 (right), contain large crystals (>2 μm), implying large diffusional paths. This, combined with the rather low surface-diffusion coefficients for zeolites (typically 10^{-8} cm^2/s), makes the exchange rather slow. The time required for the Fe species to diffuse along those channels would be days. Extending time or Fe concentration may facilitate full exchange. However, an undesired process, hydrolysis of Fe^{III} to inactive FeO_x, is competing. This situation is illustrated in Fig. 1.

Alternatively, full exchange levels can be achieved by shortening the diffusional lengths by decreasing the size of the zeolite crystals. In contrast to acid leaching, which removes framework Al [30,31], alkaline treatments preferentially extract Si, as initially reported by the Mobil Research & Development team [32–34]. Subsequently, several groups applied this technique in a more extended fashion [35–42]. There have been two major topics of interest: (i) aluminum zoning coupled with desilication and (ii) intracrystalline mesoporosity development to create hierarchical porous systems. Recently, new observations were reported [43]. We made use of the desilication effect of NaOH solutions and introduced an approach based on fracturing the crystal agglomerates of commercial zeolites. ZSM5 was fully Fe-exchanged by treating the parent zeolite with a base solution before the exchange. It demonstrated improved performance in N_2O decomposition. In this paper, the evolution of the porous structure is explored, and structural characterisation and activity measurements are used to determine the optimal leaching conditions for full exchange.

2. Experimental

2.1. Parent zeolite

The ZSM5 zeolite, acquired from Alsi Penta (AP-SM27), consists of an ammonium form with a Si/Al ratio of ca. 12 (measured by inductively coupled plasma spectroscopy [ICP]), in agreement with the commercial specifications. Chemical analysis also revealed trace amounts of iron (ca. 500 ppm). The use of commercial zeolites implies a more complex system in terms of less well-defined sample (sample history). However, its high direct applicability as a catalyst as well as a precursor for the preparation of other materials (e.g., Fe-zeolites) justifies its use.

2.2. Alkaline treatment of the samples applying NaOH solutions

The NH_4-ZSM5 zeolite was treated with an alkali solution at different conditions, followed by exchange with a NH_4NO_3 solution to recover the NH_4^+ form. Finally, iron was introduced by WIE under controlled conditions. During the alkaline treatment, the sample was subjected to a 0.2 M NaOH solution (75 ml of solution per g of zeolite). The slurry mixture was refluxed at 353 K. The procedure was carried out for two different durations (leaching time), 30 and 120 min. These durations were selected after a preliminary screening over a wider window and are representative for "mild" and "severe" conditions. The samples were filtered, washed, dried, and finally exchanged twice with 0.5 M NH_4NO_3 at 353 K for 1 h (50 ml of solution per g of zeolite).

2.3. Catalyst preparation

The incorporation of Fe was carried out by WIE on both the as-received zeolite (reference) and modified samples by alkaline treatment. Aiming for a theoretical iron loading of 2.0 wt%, the catalysts were prepared under acidic conditions (pH ca. 2.5) to avoid the precipitation of FeO_x species. After filtering, washing, and drying, the catalysts were calcined at 773 K for 4 h. The catalyst precursors (treated zeolites) and catalysts (containing Fe) are designated as AT-30 (alkali treated for 30 min) and AT-120 (alkali treated for 120 min).

2.4. Physicochemical characterisation

The chemical composition of the catalysts was determined by ICP-OES using a Perkin-Elmer Optima 3000DV (axial). Possible structural changes of the modified materials were studied by X-ray diffraction (XRD). A Cu-K_α X-ray source was used ($\lambda = 0.1541$ nm), and data were collected in the range of 5–35 (2θ, °) with a step size of 0.02° (2θ) and a counting time of 2 s (step mode operation). Fourier transform infrared (FTIR) spectra were recorded in He on a Nicolet Magna 860 Fourier transform spectrometer using a Spectratech diffuse reflectance accessory, equipped with a high-temperature cell. The sample was pretreated at 473 K for 2 h in a flow of He to remove physisorbed water and any contaminants.

Temperature-programmed reduction (TPR) with H_2 was performed in a Micromeritics TPD/TPR 2900 apparatus, using a high-purity mixture of 5 vol% H_2 in Ar to reduce the samples. Cupric oxide (Aldrich) was used for calibration. The following procedure was applied: (1) heating the samples in He at 423 K for 1 h, (2) cooling to room temperature in the same gas, (3) flushing with He for 0.5 h at room temperature to stabilize the baseline, and (4) switching to the reductive H_2/Ar mixture and starting the temperature program (at a heating rate of 10 K/min). The gas at the reactor outlet was passed through a cold trap (acetone–dry ice) to remove the water produced during the reduction before entering the thermal conductivity detector.

Temperature-programmed desorption–mass spectroscopy (TPD–MS) measurements were carried out in a Mettler Toledo system (TGA/SDTA 851E) equipped with a Thermo-Star quadrupole mass spectrometer. The sample, typically 15 mg, was stabilized in helium (60 ml/min) at 303 K for 30 min, then heated to 1073 K at a rate of 10 K/min, while continuously monitoring the fragments $m/z = 17$ (mainly NH_3 and negligible contribution of water) and 18 (H_2O).

The morphology and texture of the samples were studied by scanning electron microscopy (SEM) and N_2-physisorption. Nitrogen adsorption at 77 K was carried out in a QuantaChrome Autosorb-6B apparatus. Samples were previously evacuated at 573 K for 16 h. Surface area (S_{BET}) of the samples was calculated by the BET method [44], micropore volume (V_{micro}) was determined using the t-plot method [45], and pore size distributions of the solids were derived using the BJH method [46]. Using BET areas for zeolites is generally accepted, particularly when the comparison is done on the same structure type. SEM images were recorded with a Philips XL 20 microscope at 10 kV. The samples were coated with gold to improve contrast.

2.5. Catalytic measurements

Activity tests were carried out in a six-flow reactor system. Each run used 50 mg of catalyst particles (125–250 μm). The catalysts were tested in pure N_2O/He conditions (4.5 mbar N_2O) at a total pressure of 3 bar. Space–time was calculated as $W/F^\circ(N_2O) \approx 900$ kg s mol^{-1}, where W is the catalyst mass and $F^\circ(N_2O)$ is the molar flow of N_2O at the reactor inlet). The products were discontinuously analyzed by gas chromatography (Chrompack CP 9001) and continuously analyzed with a chemiluminescence NO-NO_2 analyzer (Ecophysics CLD 700 EL). The chromatograph was equipped with a Poraplot Q column (for N_2O and N_2/O_2 separation) and a Molsieve 5A column (for N_2 and O_2 separation). Before reaction, the catalysts were pretreated in He at 673 K for 1 h, then cooled in the same gas to the starting reaction temperature. After 1 h of operation, the concentration of the different gases was constant and thus considered steady state. Preliminary studies [47] verified the absence of diffusion limitations on the reaction rate for this reaction.

3. Results

3.1. Fe-exchange hindrance on ZSM5

Boosting the Fe-ZSM5 performance by increasing Fe loading is not straightforward, as illustrated in Fig. 2, which shows the performance of several Fe-ZSM5 catalysts. The catalysts were prepared aiming at three different iron concentrations: 0.5, 1.0, and 5.0 wt% nominal. The latter case contained an excess of Fe-salt solution (corresponding to a 250% exchange level). No activity increase was observed. The activity was about the same for the two high-iron cases (1.0 and 5.0 wt%). Elemental analysis (ICP in Table 1) indicates that the achieved Fe content in the samples was no greater than 0.9 wt%, even when using an excess of Fe-salt. This drawback is caused by the crystal size effect of ZSM5 during WIE as mentioned earlier. This is further supported with experiments using BEA and FER zeolites. As shown in Fig. 1, these zeolites contain smaller crystals and were fully exchanged (data not shown), confirming the existence of a diffusional barrier on ZSM5 for exchange.

3.2. Crystal deagglomeration and full Fe-exchange

The accessibility of the exchange sites can be improved by alkaline leaching. Applying a base solution before the ex-

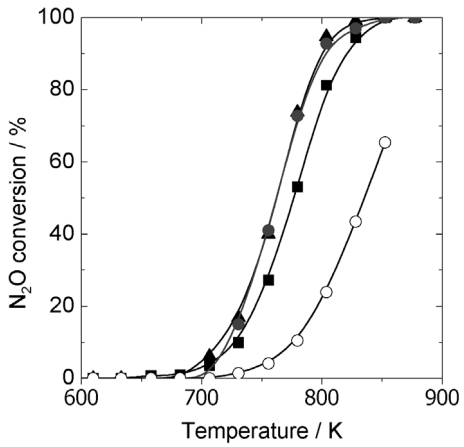

Fig. 2. Un-treated Fe-ZSM5 catalysts. Effect of the *targeted iron loading* on N_2O decomposition activity for the ZSM5 system. Reaction conditions: 4.5 mbar N_2O, He balance at 3 bara total pressure and W/F° $N_2O = 900$ kg s mol^{-1}. (○) parent ZSM5; (■) 0.5; (●) 1.0 and (▲) 5.0 wt% Fe.

Table 1
Summary of exchange levels and Si/Al ratios derived from ICP-OES analyses

Sample	Fe (wt%) (target)	Fe (wt%) ICP	Exchange[c] (%)	Si/Al (mol/mol)
ZSM5 as-received	–	468[a]	2.2	12.5
0.5Fe-ZSM5	0.50	0.47	23.2	12.8
1.0Fe-ZSM5	1.00	0.90	46.3	12.7
5.0Fe-ZSM5	5.00	0.86	35.8	13.4
Fe-AT-30[b]	2.00	1.93	101.8	13.0
Fe-AT-120[b]	2.00	1.98	100.5	10.9

[a] In parts per million (ppm).
[b] AT means alkaline treated.
[c] As $(Fe/Al)_{ICP} \times 300$.

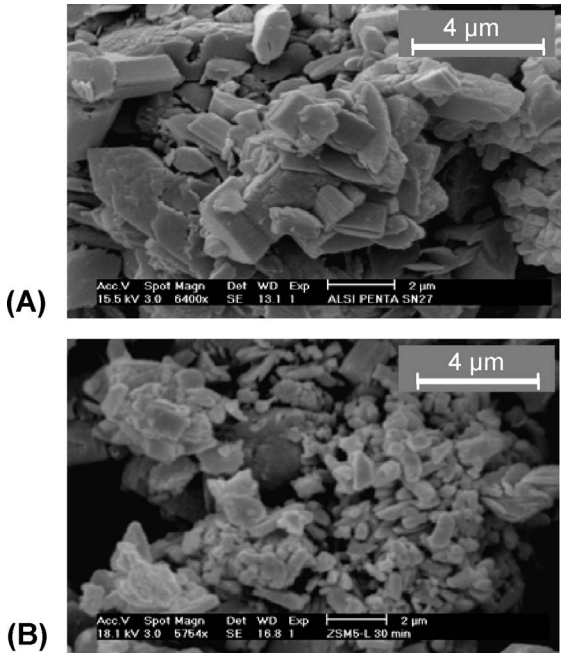

Fig. 3. SEM pictures of ZSM5 samples: (A) parent ZSM5 and (B) alkali treatment 30 min (AT-30).

change provokes desilication while leaving the Brønsted sites unchanged. This was concluded earlier based on NH_3-TPD experiments [40] and FTIR measurements in the OH-stretching region [48] showing that controlled alkaline treatment generally preserved zeolite acidity. Deagglomeration of the crystals is also expected to occur, as earlier confirmed by SEM. Fig. 3 presents the most relevant SEM results. The as-received material (case A) presents agglomerates of large (2–4 µm) crystals. A significant change is observed on alkaline treatment (case B), with large crystals broken down into smaller ones, with particles <1 µm visible. Similar results were obtained for the AT-120 material.

Alkaline treatment did not lead to any dramatic structural changes, as revealed by XRD. Fig. 4 shows the XRD patterns of the ZSM5 samples before and after alkaline leaching. Although the intensity of the reflections was decreased considerably, the MFI lattice was preserved at long-order range. The reduced intensities, also observed elsewhere [40,41], are consistent with the smaller particle size detected by SEM.

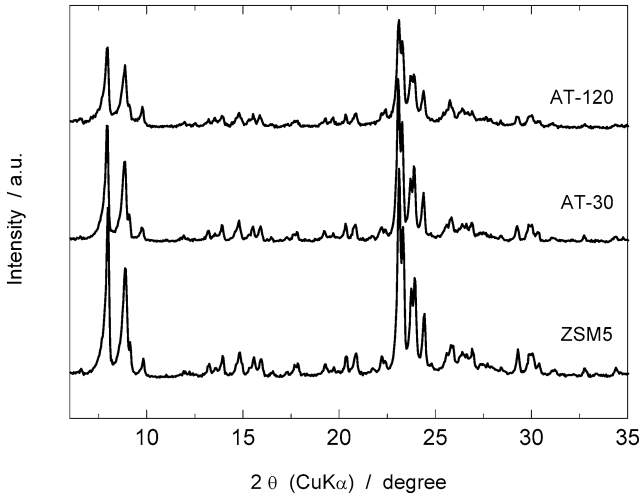

Fig. 4. XRD patterns of ZSM5. Effect of alkali treatment time.

Table 2
Crystallinity loss estimation for different treatment times

Sample	Crystallinity[a] (%)	Crystallinity reduction (%)
ZSM5 as-received	100	–
Fe-AT-30	66	34
Fe-AT-120	42	58

[a] Based on the intensity of the reflection at $2\theta = 7.94°$ corresponding to the (011) plane.

Table 2 gives a rough calculation of the crystallinity loss on leaching time. This is an indicative calculation taking the most intense peak as a reference [2θ Cu-$K_\alpha = 7.94°$, corresponding to the (011) plane]. For the severe treatment (AT-120), the crystallinity of the zeolite decreased by >50%, and some intensity ratios changed with respect to the parent sample.

SEM results indicate that deagglomeration occurs, and that the diffusional limitations of Fe^{III} during WIE could be sufficiently eliminated to allow full exchange. At such conditions, Fe exchange is facilitated, as confirmed by ICP measurements on the Fe loadings (Table 1) showing that full Fe^{III} exchange values are achieved on alkaline leaching.

Examining the Si/Al ratio is also essential to gaining a better understanding of the processes involved. Although the Si/Al ratio for AT-30 remained fairly constant, a reduction can be observed for the prolonged leaching time sample (Fe-AT-120). A decrease of around 15% means that a fraction of silicon was extracted during treatment while aluminium was left in the structure. Thus the exchange capacity of the material increases per unit of weight. These results on leaching are in agreement with the literature [32–42].

Based on the ICP results, two major conclusions can be drawn:

1. A fully exchanged Fe^{III}-ZSM5 zeolite can be prepared on mild alkaline pretreatment. The improved activity of this material is apparently related to a higher amount of Fe loaded in the zeolite matrix.
2. The Si/Al ratio decreases only after prolonged treatment.

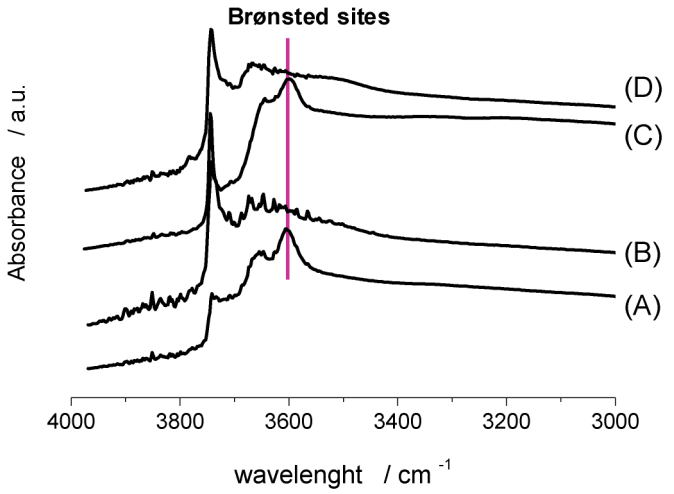

Fig. 5. Infrared spectra of the OH stretching region of the sample after various treatments. Spectra taken at 473 K after outgassing. (A) H-form ZSM5 obtained by calcination of the NH_4-form at 823 K, (B) alkaline treated ZSM-5 (Na-form), (C) NH_4NO_3 exchange + calcination, (D) Fe-AT-30 catalyst.

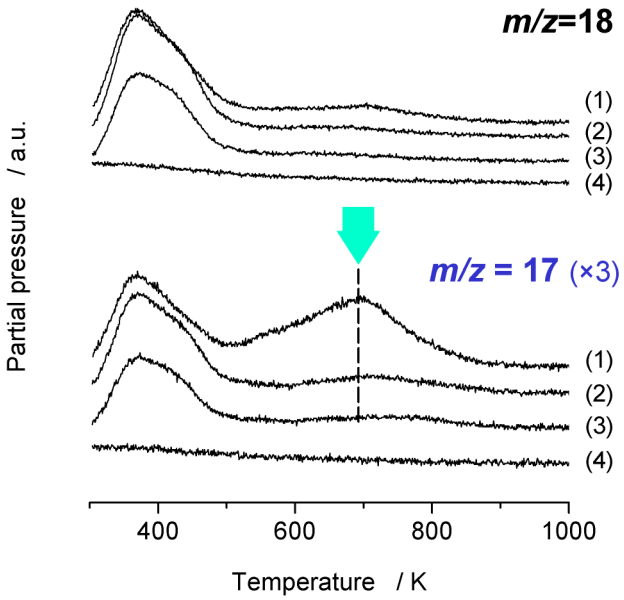

Fig. 6. TPD-MS of the samples upon thermal treatment in helium. Fragments $m/z = 17$ (essentially NH_3 and a negligible contribution of H_2O) and 18 (H_2O) were monitored continuously. Samples: (1) starting NH_4-ZSM5 zeolite, (2) Fe-AT30, (3) Fe-AT120 and (4) blank experiment. Both samples (2) and (3) refer to the catalysts after Fe-exchange but before calcination. Conditions: pure helium; ramp 10 K min^{-1}. Traces of $m/z = 17$ were amplified (×3) to improve clarity.

Diffuse reflectance Fourier transform infrared spectroscopy analysis of the Brønsted sites gave further evidence of full exchange. The OH-stretching region was monitored on the various treatments. As shown in Fig. 5, the following events occur: disappearance of the adsorption band at 3610 cm^{-1}, characteristic of Brønsted acid sites [49] on alkaline treatment due to the full exchange with Na^+ (B); full recovery of the band on ion exchange with NH_4NO_3 and subsequent calcination (C); and final disappearance of the band on Fe^{III} exchange (D). This proves that indeed Fe is responsible for the disappearance of the absorption band at 3610 cm^{-1}. The increased silanol band at 3740 cm^{-1} on treatment results from the larger external surface area on treatment. Interestingly, no distinct signs of additional extra-framework Al species were observed in the alkaline-modified samples, in agreement with the preferential desilication effect on caustic washing.

Full exchange was complimented by TPD-MS studies. If full exchange were not achieved, then ammonia (from ammonium groups) would be released from the sample on thermal treatment, as the Fe^{III} exchange was performed in the NH_4-modified samples. The samples were heated in He while continuously monitoring the $m/z = 17$ and 18 fragments. As seen in Fig. 6, only the starting zeolite contained noticeable NH_4^+ groups. For the Fe-AT cases, small and broad NH_3 peaks can be seen that quantitatively correspond to 7 and 5% of initial NH_4^+ for Fe-AT-30 and -120, respectively. Thus, the true exchange level lies between 93 and 95%, which is close to full exchange. Based on the targeted Fe concentration of 2 wt%, the expected exchange degree indeed corresponds to a 95% exchange.

TPR reveals the reductive character of the Fe species and also confirms the full Fe exchange achieved. The TPR profiles are presented in Fig. 7B. Two catalysts of the untreated samples were included for comparison (A). The base-leached samples show a reduction peak around 700 K attributed to Fe^{III}-to-Fe^{II} reduction in exchanged positions of zeolites [27,50,51]. A very small contribution around 900–950 K was observed especially for the AT-30, due to traces of FeO_x. In contrast, the untreated samples contain a large proportion of FeO_x. This assignment of FeO_x peak is based on H_2-reductive experiments with Fe_2O_3 reported earlier [27]. The FeO_x species comprise all possible Fe species thermodynamically predicted from nitrate solutions, including amorphous Fe hydroxide, hematite (α-Fe_2O_3) and goethite (α-FeO(OH)) [52].

Table 3 summarises the quantitative analysis of the TPR measurements. Both the total H_2 consumption in the TPR, expressed as H_2/Fe, and the proportion of FeO_x were estimated. The H_2/Fe ratio for the modified samples remained close to 0.5, the stoichiometric value for the Fe^{III}-to-Fe^{II} step, but increased for the unmodified samples containing large proportions of FeO_x. The amount of FeO_x can be roughly calculated by deconvoluting the profile in different peaks (see the estimates in Table 3) and taking into account a low-temperature contribution of FeO_x at 700 K (hematite to magnetite) corresponding to 1/8 of the high-temperature contribution (magnetite to Fe^0), while the overall reduction of FeO_x consumes a H_2/Fe ratio of 1.5. The treated catalysts contain a very small fraction of FeO_x clusters, ca. 1% of the total Fe, meaning that virtually all of the iron is present as exchanged species. The profiles for the untreated samples in Fig. 7A indicate large proportions (ca. 15–30%) of FeO_x.

3.3. Textural changes on base treatment

It has been demonstrated that NaOH treatment is beneficial in terms of improving exchange for Fe-ZSM5. Both treatment times (AT-30 and AT-120) showed similar trends in terms of exchange degree. This section reports a thorough study of porosity

Table 3
Summary of TPR analysis of the catalysts

Sample	Fe (wt%) (target)	Fe (wt%) ICP	H_2/Fe			FeO_x[a] (%)	Fe[b] (wt%) exch.
			$LT_{(ca.\ 700\ K)}$	$HT_{(ca.\ 900\ K)}$	Total		
0.5Fe-ZSM5	0.50	0.47	0.410	0.350	0.760	27	0.3
5.0Fe-ZSM5	5.00	0.86	0.460	0.210	0.670	15	0.5
Fe-AT-30	2.00	1.93	0.400	0.005	0.400	< 1	1.9
Fe-AT-120	2.00	1.98	0.490	0.005	0.490	< 1	2.0

[a] % FeO_x respect to the total Fe, as a rough calculation by the equation below. It is assumed that the low-temperature contribution for FeO_x corresponds to 1/8th of the HT:

$$(Fe_2O_3)_{clusters} = \frac{(1+1/8)HT}{1.5} \Big/ \left[\frac{(1+1/8)HT}{1.5} + \frac{LT - 1/8HT}{0.5}\right].$$

[b] Values between parenthesis wt% of exchanged Fe: Fe(ICP) × (100 − % FeO_x).

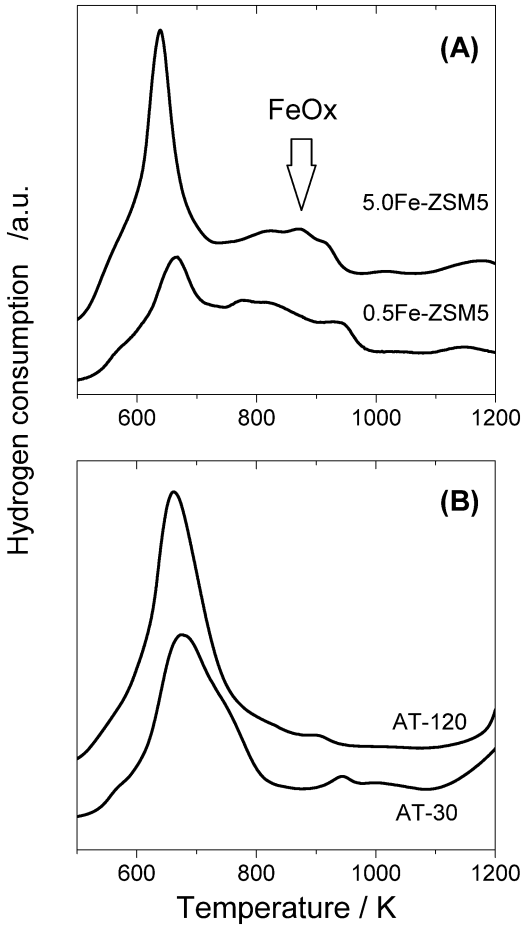

Fig. 7. H_2-TPR profiles of the Fe-ZSM5 systems: (A) from the parent ZSM5 and (B) from alkali treated ZSM5. Conditions: 5% H_2/Ar; ramp 10 K min^{-1}.

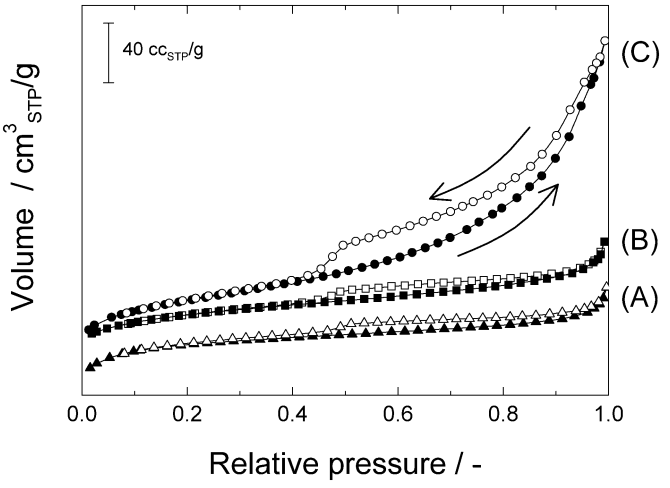

Fig. 8. N_2 adsorption isotherms at 77 K of alkaline-treated ZSM5 samples (AT-30 & AT-120) as well as the starting zeolite.

Table 4
Surface areas and pore volumes of Fe-ZSM5 catalysts before and after alkali treatment

Sample	S_{BET}[a] (m^2/g)	V total (cm^3/g)	V micro (cm^3/g)	S_A meso (m^2/g)	S_A micro (m^2/g)
ZSM5 as-received	405	0.21	0.16	35	370
Fe-AT-30	336	0.20	0.12	54	282
Fe-AT-120	364	0.38	0.09	135	229

[a] For comparison between the samples, the specific surface area was determined by the BET method, even this method has no physical meaning for microporous zeolites.

evolution (textural changes) based on N_2 physisorption analysis.

Fig. 10 shows the N_2 adsorption and desorption isotherms of the parent sample and AT samples. The isotherm of the ZSM5 sample is characteristic of microporous materials with a plateau at high relative pressures (type I, IUPAC). It also contains some minor mesoporosity and macroporosity effects. In general, microporosity prevails in the modified samples, as can be derived from the high uptake of N_2 at low relative pressures (<0.1). The isotherm of AT-30 is rather similar to that of the starting material; however, the adsorption behaviour of AT-120 indicates noticeable hysteresis at high p/p_0 values, related to the creation of mesopority in the intraparticle space of the zeolite. The N_2 isotherm is transformed from type I to combined types I and IV with pronounced hysteresis. The largely parallel disposition of the adsorption and desorption branches of the loop suggests, in contrast to cavities, the presence of open mesopores connected to the outer surface [53]. The presence of both microporosity and mesoporosity in AT-120 is confirmed by the t-plot results compiled in Table 4.

Table 4 shows the adsorption parameters of the samples. For AT-30, the majority of the surface area arises from the

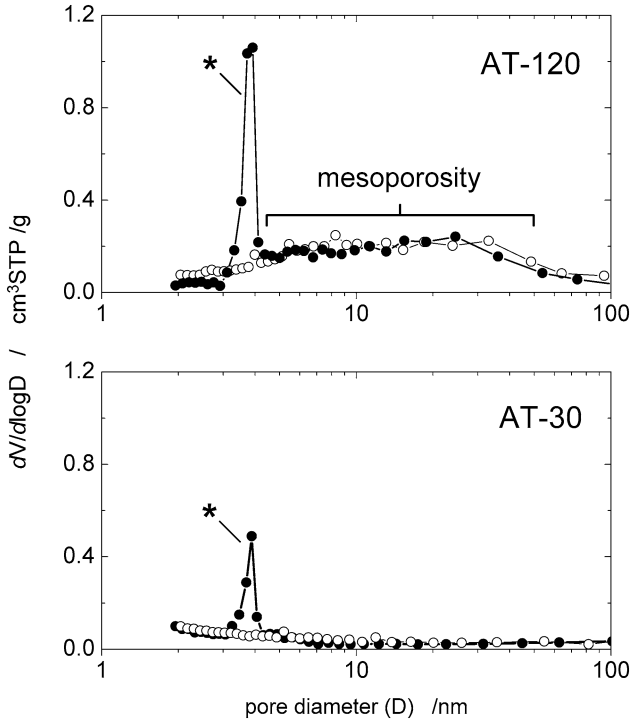

Fig. 9. BJH pore size distribution derived from N_2-adsorption (●) and desorption (○) isotherms for the modified samples. Asterisk indicates TSE effect.

micropores, with only a small fraction of mesoporosity created. Although argon physisorption was not done to evaluate microporosity, values in Table 4 for AT-30 indirectly reveal that the micropores are affected (ca. 25% reduction in terms of micropore volume). The mesopore size distribution given in Fig. 8 (bottom) shows no mesoporosity development until 100 nm. The increase in mesopore area (from 35 to 54 m^2/g) likely results from the newly formed interparticle area (originating from the deagglomeration) at dimensions >0.1 μm. This is consistent with the AT-30 crystal sizes <1 μm observed on SEM. Moreover, because the reduced micropore volume is not accompanied by substantial mesopore development, the diminution can be ascribed to both pore blockage during the defragmentation process and the formation of smaller crystal domain sizes, which typically have smaller micropore volumes [54].

The pore size distribution of the AT-120 sample includes a wide range of mesopores (4–50 nm). The *t*-plot analyses indicate that the mesopore contribution to the total area is enhanced significantly, by almost 400% of the original value (Table 4). Additionally, whereas the total pore volume remains constant between AT-30 and ZSM5, the value for AT-120 increases considerably (from 0.20 to 0.38 cm^3/g). Much void space has been formed, leading to a less-dense solid. In addition, for AT-120, it can be concluded that even though micropore volume decreases after treatment, micropore size should remain unaffected, as has been reported for other commercial ZSM-5 zeolites [41,48] based on high-resolution, low-pressure Ar adsorption measurements.

The type of hysteresis (H_3) indicates "slit pores." However, a broad distribution of randomly organized mesopores will often result in an H_3-type hysteresis loop, indeed suggesting slit-shaped geometry even when the pores have a different geometry. This is particularly true when pore size crosses the critical 4-nm size range, leading to an emphasized lower closure point of the hysteresis loop. In previous work [55] we visualized an ill-defined geometry of the pores, with a broad distribution of pore sizes, but far from slit-shaped.

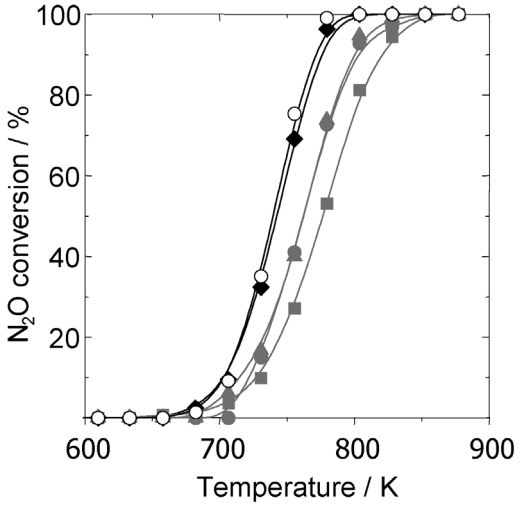

Fig. 10. N_2O decomposition experiments. Effect of the alkaline leaching on the base promoted catalysts: (◆) Fe-AT-30 and (○) Fe-AT-120. Reaction conditions: 4.5 mbar N_2O, He balance at 3 bara total pressure and W/F° $N_2O = 900\ kg\,s\,mol^{-1}$. Grey symbols correspond to data in Fig. 2.

Finally, it is worth mentioning that analysis of the desorption branch on these materials can lead to misinterpretation of the physical reality of the samples. An intense peak at ca. 3.8–3.9 nm (Fig. 8) is due to the tensile strength effect (TSE) [53,56,57]. TSE appears as a forced closure of the hysteresis loop due to a sudden drop in the adsorbed volume along the desorption branch in the p/p_0 range of 0.41–0.48. The physical nature is related to the increased tensile strength in the adsorbed phase. More details on this have been provided previously [57].

3.4. N_2O decomposition activity measurements

The activity of the AT catalysts, together with the untreated samples for comparison, was tested in N_2O decomposition (Fig. 9). The alkaline treatment noticeably increased performance. The Fe-AT-30 and Fe-AT-120 samples had very similar activity levels. Prolonged treatment had no further effect on the catalytic properties.

Knowledge of the actual proportion of Fe^{III} exchanged is essential to interpreting the activity trends. The activity in the N_2O decomposition reaction is related not to the total amount of iron (i.e., total area of the TPR peaks), but rather mostly to the exchanged species located at 600–750 K. At higher temperatures, relatively inactive Fe-oxide is reduced, as shown on TPR. Combining the chemical analysis and TPR results can provide a rough estimate of the wt% of Fe in exchanged positions (Table 3). It appears that the activity improvement results from increased Fe loading in Brønsted positions.

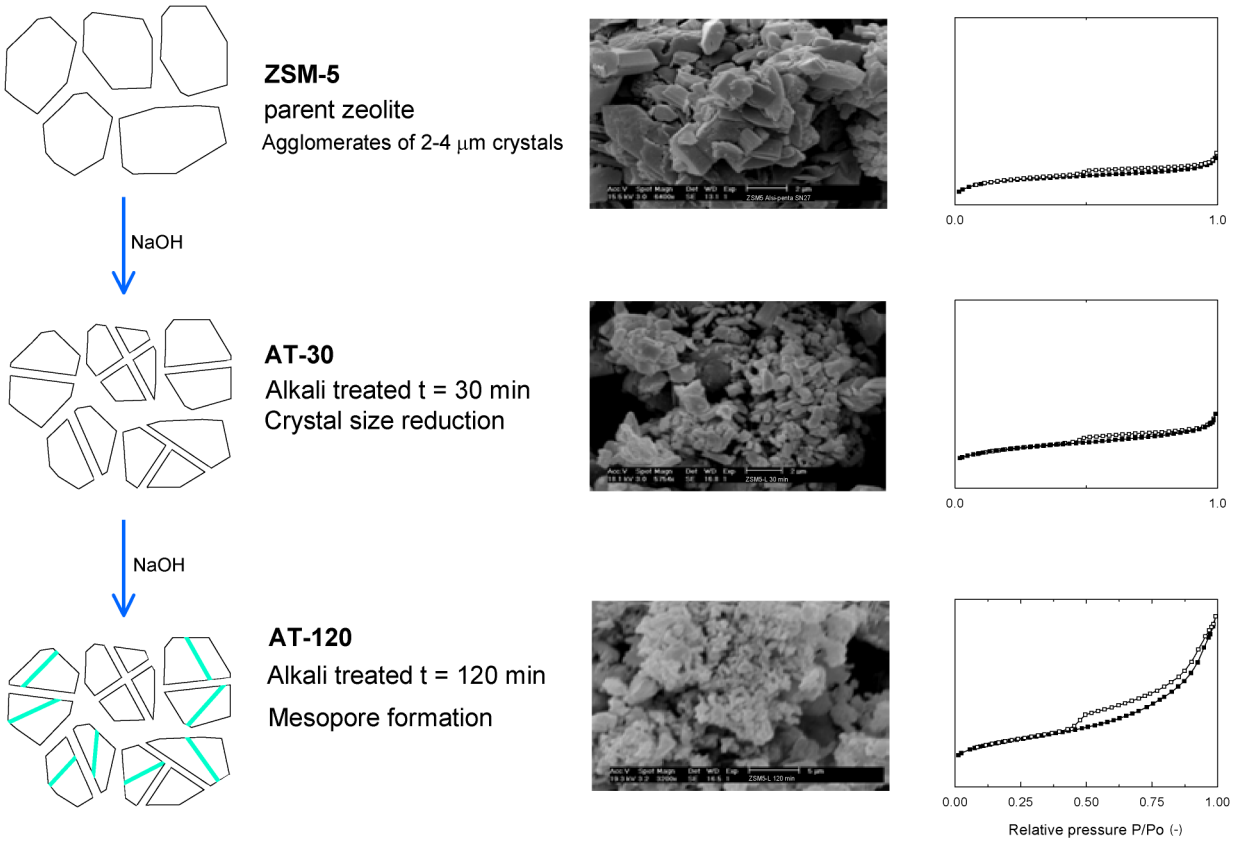

Fig. 11. Evolution of the sample's morphology upon caustic leaching.

4. Discussion

The efficient use of the Brønsted sites during Fe WIE has been explored by several research groups. Van den Brink et al. [27] used concentrated solutions of Fe^{II}–Mohr's salt and prolonged time; nevertheless, large amounts of FeO_x were formed that partially blocked the micropores after calcination, as discussed by Bitter et al. [28]. The first systematic work on the effect of the exchange level of Fe-ZSM5 was carried out by Yamada et al. [26], who achieved different Fe exchange levels but did not explain in detail how they did so. They achieved no exchange level >80%, confirming the aforementioned complexity of Fe-ZSM5.

It is clear that diffusional control occurred during exchange, and that the process could be performed for a prolonged time (days). The simultaneous hydrolysis of Fe^{III} occurred, and inactive species were formed. Even though the exchange was carried out in acidic medium (pH = 2.5), hydrolysis was still considerable. This is evidenced by TPR findings showing significant FeO_x (ca. 15–30%) for the untreated Fe-ZSM5 samples. According to thermodynamic predictions (in homogeneous solution), the extent of Fe^{III} hydrolysis should be <3% (for 0.002 M total Fe); however, TPR demonstrated larger proportions of FeO_x. This can be explained by the local pH effect in the zeolite pores. As documented in the literature [25,58], electrostatic restrictions in the microchannels and cavities induce water dissociation of the coordinated water, giving rise to hydrolysed species,

$$\begin{aligned}\left[Fe(H_2O)_6\right]^{3+} &\rightarrow H^+ + 5H_2O + Fe(OH)^{2+} \\ &\rightarrow [\cdots] \rightarrow Fe(OH)_x. \end{aligned} \quad (1)$$

As long as the Fe species are not exchanged, they slowly hydrolyse, leading to pore blocking. Thus, extending the exchange time is not an appropriate approach to accomplishing full exchange on large-crystal zeolites. We applied alkaline leaching before Fe^{III} WIE to reduce the diffusional lengths by cracking the crystal agglomerates.

The morphological and textural changes induced to the samples during desilication are summarized in Fig. 11. The starting material consisted of relatively large crystals of a commercial ZSM5 sample (Fig. 11, top). On short time treatment (AT-30), the sample underwent an initial transformation in which the crystal size was reduced considerably, leading to a slight increase in mesopore surface area. This refers to the newly intercrystalline region created, which cannot be readily deduced by examining the total BET area, because micropores are reduced from 0.16 to 0.12 cm^3/g. Because this decrease is not accompanied by the development of substantial mesoporosity, the micropore reduction is likely due to pore blockage or to formation of smaller crystal domain sizes, which typically have smaller micropore volumes. The Si/Al ratio remained fairly close to the original value (starting zeolite), suggesting that deagglomeration involves similar dissolution of both Si and Al. Based on the multitechnique approach, a short treatment time (30 min for

the particularly applied conditions of concentration and temperature) is sufficient to complete the Fe^{III} WIE and subsequently enhance the activity for N_2O decomposition.

At longer treatment time (AT-120), the same range of particle sizes as for AT-30 was visualized by SEM (Fig. 11); however, a network of mesopores with a wide range of sizes was created, while the MFI topology remained well preserved. The creation of mesopores had no effect on the exchange process or on the reaction. Obviously, it does not favour the exchange, because full exchange was already achieved at the shorter treatment time (Fe-AT-30). During reaction, mesoporosity appears to be irrelevant for N_2O decomposition. This is because the mesopores created in reduced crystals do not further enhance the diffusion of N_2, O_2, and N_2O molecules, being relatively small compared with the pore dimensions and small crystals (short diffusion path lengths).

Some mechanistic information on desilication can be extracted from the data. The results indicate that the early stage before mesoporosity development implies cracking of the zeolite crystals. This may be related to the amount of Al present in the sample, that is, the Si/Al ratio. Ogura et al. [37] proposed an intercrystalline mechanism of leaching by removing amorphous SiO_x groups between twin grains. Groen et al. suggested an intracrystalline character of the mesoporosity based on their results [40–42,48,55], supported by the work of Subotic-Čižmek et al. [36] on dissolution of high-silica zeolites in alkaline conditions. Studies on desilication are commonly based on high-silica zeolite (Si/Al = 20–600) or even pure silicalite. In this study a very rich-aluminium zeolite was used (Si/Al = 12), because Fe^{III} species must be exchanged on the Brønsted sites originated by Al substitution. Bonds formed by Si–O–Al generally are weaker and less stable than those formed by Si–O–Si [30,59]. Such bonds provide instability to the framework and can be easily attacked/hydrolysed. However, this holds for acid leaching; in the case of base treatment, it was recently shown that framework Al gives stability against desilication [48]. Therefore, the breakdown process is understood as a massive dislodgement of the crystal agglomerates by removing the more amorphous parts or weakest spots, involving both Si and Al removal. For instance, the boundaries of the intergrown crystals (as shown in Fig. 3A) are weak spots where the NaOH would first attack; this provokes deagglomeration.

As for the catalytic reaction, the improved activity of this material was first related to a larger proportion of exchanged Fe^{III} (as revealed by ICP and TPR). Breaking down the agglomerates at mild conditions improves Fe exchange in the liquid phase. In reaction, more Fe sites are available for the gas phase. However, comparing the activity increase at, say, 750 K, clearly shows that a fourfold increase in Fe exchange corresponds to a twofold improvement in performance. From this comparison, it can be concluded that only a fraction of the extra Fe becomes active, with the amount increasing with the degree of exchange. Part of the Fe becomes a reaction spectator.

Designing a catalyst containing just the most active Fe species is a difficult task, because only macroscopic variables (far from the atomic level), such as [Fe], temperature, and pH, are manipulated. Also, it is reasonable to consider that when operating at levels close to the full exchange capacity, the formation of isolated Fe species (less active) is preferred, because an insufficient number of Brønsted sites are available. Therefore, a complex mixture of different (active) species is created. However, even though stoichiometric-linear activity improvements are not achieved (in line with the loading increase), this approach is worth attempting, because Fe salts are cheap and the method is relatively simple.

5. Conclusion

The crystal size of the zeolite ZSM5 dominates the kinetics of Fe^{III} exchange during preparation. The large crystal size makes its complete exchange difficult due to diffusional control.

On controlled caustic washing before WIE, ZSM5 is fully Fe^{III}-exchanged, with negligible FeO_x formation after calcination. This is achieved by controlling the size of the primary crystals of the zeolite through desilication, thereby enhancing the material's accessibility.

Applying alkaline leaching results in two phenomena. At a short treatment time (30 min), the zeolite agglomerates are reduced into smaller grains (deagglomeration). Removal of the more amorphous or weakest parts (i.e., intergrowing crystals at the boundaries of the primary crystals) may be responsible for this early-stage fragmentation. At prolonged treatment time (120 min), mesopore formation also occurs. The pore size distribution is wide (5–50 nm), but this is not relevant for either the exchange process during preparation or the subsequent N_2O reaction. The alkali-modified samples exhibit considerably enhanced N_2O decomposition activity. Based on the activity increase, we can conclude that only a fraction of the extra Fe becomes active, with the amount increasing with the degree of exchange.

Acknowledgments

I.M.C. was supported by a post-doctoral fellowship (contract HPMF-CT-2002-01873) from the European Commission (Marie Curie Actions). The authors thank Niek v/d Pers for providing technical support.

References

[1] J. Valyon, V.S. Millman, W.K. Hall, Catal. Lett. 24 (1994) 215.
[2] Y.F. Chang, J.G. McCarty, Y.L. Zhang, Catal. Lett. 34 (1995) 163.
[3] F. Kapteijn, G. Mul, G. Marbán, J. Rodríguez-Mirasol, J.A. Moulijn, Stud. Surf. Sci. 101 (1996) 641.
[4] F. Kapteijn, G. Marbán, J. Rodríguez-Mirasol, J.A. Moulijn, J. Catal. 167 (1997) 256.
[5] C. Pophal, T. Yogo, K. Tanabe, K. Segawa, Catal. Lett. 44 (1997) 271.
[6] C. Pophal, T. Yogo, K. Yamada, K. Segawa, Appl. Catal B 16 (1998) 177.
[7] M. Mauvezin, G. Delahay, F. Kisslich, B. Coq, S. Kieger, Catal. Lett. 62 (1999) 41.
[8] G.I. Panov, A.K. Uriarte, M.A. Rodkin, V.I. Sobolev, Catal. Today 41 (1998) 365.
[9] X.B. Feng, W.K. Hall, Catal. Lett. 41 (1996) 45.
[10] X.B. Feng, W.K. Hall, J. Catal. 166 (1997) 368.
[11] M. Kogel, V.H. Sandoval, W. Schwieger, A. Tissler, T. Turek, Catal. Lett. 51 (1998) 23.

[12] M. Kogel, R. Monning, W. Schwieger, A. Tissler, T. Turek, J. Catal. 182 (1999) 470.
[13] R.Q. Long, R.T. Yang, J. Am. Chem. Soc. 121 (1999) 5595.
[14] W.K. Hall, X.B. Feng, J. Dumesic, R. Watwe, Catal. Lett. 52 (1998) 13.
[15] H.Y. Chen, W.M.H. Sachtler, Catal. Today. 42 (1998) 73.
[16] H.Y. Chen, W.M.H. Sachtler, Catal. Lett. 50 (1998) 125.
[17] H.Y. Chen, T.V. Voskoboinikov, W.M. H Sachtler, J. Catal. 180 (1998) 171.
[18] H.Y. Chen, T.V. Voskoboinikov, W.M. H Sachtler, J. Catal. 186 (1999) 91.
[19] T.V. Voskoboinikov, H.Y. Chen, W.M. H Sachtler, Appl. Catal. B 19 (1998) 279.
[20] P. Marturano, L. Drozdová, A. Kogelbauer, R. Prins, J. Catal. 192 (2000) 236.
[21] P. Marturano, L. Drozdová, G.D. Pirngruber, A. Kogelbauer, R. Prins, Phys. Chem. Chem. Phys. 3 (2001) 5585.
[22] M. Rauscher, K. Kesore, R. Monnig, W. Schwieger, A. Tissler, T. Turek, Appl. Catal. A 184 (1999) 249.
[23] R.W. Joyner, M. Stockenhuber, Catal. Lett. 45 (1997) 15.
[24] P. Marturano, A. Kogelbauer, R. Prins, Stud. Surf. Sci. Catal. 125 (1999) 619.
[25] P. Marturano, A. Kogelbauer, R. Prins, J. Catal. 190 (2000) 460.
[26] K. Yamada, S. Kondo, K. Segawa, Microporous Mesoporous Mater. 35–36 (2000) 227.
[27] R.W. van den Brink, S. Booneveld, J.R. Pels, D.F. Bakker, M.J.F.M. Verhaak, Appl. Catal. B 32 (2001) 73.
[28] J.H. Bitter, A.A. Battiston, S. van Donk, K.P. de Jong, D.C. Koningsberger, Microporous Mesoporous Mater. 64 (2003) 175.
[29] J. Pérez-Ramírez, F. Kapteijn, G. Mul, J.A. Moulijn, Chem. Commun. (2001) 693.
[30] H.K. Beyer, in: H.G. Karge, J. Weitkamp (Eds.), Molecular Sieves, Science and Technology. Post-Synthesis Modifications I, Springer, Berlin, 2002, p. 20.
[31] S. van Donk, A.H. Janssen, J.H. Bitter, K.P. de Jong, Catal. Rev. Sci. Technol. 45 (2003) 297.
[32] G.T. Kokotailo Jr., A.C. Rohrman, US Patent 4,703,025 (1987).
[33] R.M. Dessau, E.W. Valyocsik, N.H. Goeke, Zeolites 12 (1992) 776.
[34] R.M. Dessau, E.W. Valyocsik, N.H. Goeke, in: J.B. Higgins, R. van Ballmoos, M.M. Treacy (Eds.), Proceedings of the 9th International Zeolite Conference, Extended Abstracts and Program, Butterworth–Heinemann, Stoneham MA, 1992, RP96.
[35] L. Aouali, J. Jeanjean, A. Dereigne, P. Tougne, D. Delafosse, Zeolites 8 (1988) 517.
[36] (a) A. Cizmek, L. Komunjer, B. Subotic, M. Siroki, S. Roncevic, Zeolites 11 (1991) 258;
(b) A. Cizmek, L. Komunjer, B. Subotic, M. Siroki, S. Roncevic, Zeolites 11 (1991) 810;
(c) A. Cizmek, L. Komunjer, B. Subotic, M. Siroki, S. Roncevic, Zeolites 12 (1992) 190;
(d) C. Kosanovic, B. Subotic, V. Kaucic, M. Skreblin, Phys. Chem. Chem. Phys. 2 (2000) 3447;
(e) A. Cizmek, L. Komunjer, B. Subotic, R. Aiello, F. Crea, A. Nastro, Zeolites 14 (1994) 182;
(f) A. Cizmek, B. Subotic, R. Aiello, F. Crea, A. Nastro, C. Tuoto, Microporous Mater. 4 (1995) 159;
(g) A. Cizmek, B. Subotic, I. Smit, A. Tonejc, R. Aiello, F. Crea, A. Nastro, Microporous Mater. 8 (1997) 159.
[37] M. Ogura, S. Shinomiya, J. Tateno, Y. Nara, M. Nomura, E. Kikuchi, M. Matsukata, Appl. Catal. A 219 (2001) 33.
[38] H. Matsuura, N. Katada, M. Niwa, Microporous Mesoporous Mater. 66 (2003) 283.
[39] L.L. Su, L. Liu, J. Zhuang, H.X. Wang, Y.G. Li, W.J. Shen, Y.D. Xu, X.H. Bao, Catal. Lett. 91 (2003) 155.
[40] J.C. Groen, L.A.A. Peffer, J.A. Moulijn, J. Pérez-Ramírez, Microporous Mesoporous Mater. 69 (2004) 29.
[41] J.C. Groen, L.A.A. Peffer, J.A. Moulijn, J. Pérez-Ramírez, Colloid Surf. A 241 (2004) 53.
[42] J.C. Groen, J.C. Jansen, J.A. Moulijn, J. Pérez-Ramírez, J. Phys. Chem. B 108 (2004) 13062.
[43] I. Melián-Cabrera, S. Espinosa, C. Mentruit, F. Kapteijn, J.A. Moulijn, Catal. Commun. 7 (2005) 100.
[44] S. Brunauer, P.H. Emmet, E.J. Teller, J. Am. Chem. Soc. 60 (1938) 309.
[45] B.C. Lippens, J.H. de Boer, J. Catal. 4 (1965) 319.
[46] E.P. Barrett, L.G. Joyner, P.P. Halenda, J. Am. Chem. Soc. 73 (1951) 373.
[47] J. Pérez-Ramírez, R.J. Berger, G. Mul, F. Kapteijn, J.A. Moulijn, Catal. Today 60 (2000) 93.
[48] J.C. Groen, L.A.A. Peffer, J.A. Moulijn, J. Pérez-Ramírez, Chem. Eur. J. 11 (2005) 4983.
[49] A. Zecchina, S. Bordiga, G. Spoto, D. Scarano, G. Petrini, G. Leofanti, M. Padovan, J. Chem. Soc., Faraday Trans. 88 (1992) 2959.
[50] M. Mauvezin, G. Delahay, B. Coq, S. Kieger, J.C. Jumas, J. Olivier-Fourcade, J. Phys. Chem. B 105 (2001) 928.
[51] A. Guzmán-Vargas, G. Delahay, B. Coq, Appl. Catal. B 42 (2003) 369.
[52] C.M. Flynn, Chem. Rev. 84 (1984) 31.
[53] J.C. Groen, J. Pérez-Ramírez, Appl. Catal. A 268 (2004) 121.
[54] M.A. Camblor, A. Corma, S. Valencia, Microporous Mesoporous Mater. 25 (1998) 59.
[55] J.C. Groen, T. Bach, U. Ziese, A.M. Paulaime-van Donk, K.P. de Jong, J.A. Moulijn, J. Perez-Ramirez, J. Am. Chem. Soc. 127 (2005) 10792.
[56] S.J. Gregg, K.S.W. Sing, Adsorption, Surface Area and Porosity, second ed., Academic Press, London, 1982.
[57] J.C. Groen, L.A.A. Peffer, J. Pérez-Ramírez, Microporous Mesoporous Mater. 60 (2003) 1.
[58] J.W. Ward, in: J.A. Rabo (Ed.), Zeolite Chemistry and Catalysis, vol. 171, Am. Chem. Soc., Washington DC, 1976.
[59] M. Guisnet, J.-P. Gilson (Eds.), Zeolites for Cleaner Technologies, Catalytic Science Series, vol. 3, Imperial College Press, London, 2002.